Propagation of ripples on pyrochlore induced by ion beam bombardment

Qiangmin Wei,[1] Jie Lian,[2] L. A. Boatner,[3] L. M. Wang,[1,4,*] and R. C. Ewing[1,4,5]
[1]*Department of Materials Science and Engineering, University of Michigan, Ann Arbor, Michigan 48109, USA*
[2]*Department of Mechanical, Aerospace and Nuclear Engineering, Rensselaer Polytechnic Institute, Troy, New York 12180, USA*
[3]*Oak Ridge National Laboratory, Oak Ridge, Tennessee 37831, USA*
[4]*Department of Nuclear Engineering and Radiological Science, University of Michigan, Ann Arbor, Michigan 48109, USA*
[5]*Department of Geological Sciences, University of Michigan, Ann Arbor, Michigan 48109, USA*
(Received 3 December 2008; revised manuscript received 1 July 2009; published 12 August 2009)

The morphological evolution of ripples formed on the surface of $Cd_2Nb_2O_7$ pyrochlore single crystals by focused ion beam bombardment was investigated using *in situ* electron microscopy. At high ion fluences and off-normal bombardment angles, faceted surface ripples with a "terracelike" structure were observed. The ripple propagation direction was oriented along the projected ion beam direction at incident angles ranging from 35 to 65° under high-dose ion bombardment. One side of the terrace was found to be perpendicular to the incident ion beam direction, while the other side was parallel to the ion beam. The terrace propagation velocity and direction were determined and interpreted on the basis of this asymmetric structure. A model based on the propagation of a shock wave that effectively "self-selects" a stable slope was developed in order to explain the observed faceted ripple formation.

DOI: 10.1103/PhysRevB.80.085413 PACS number(s): 68.35.B−, 81.65.Cf, 79.20.Rf

I. INTRODUCTION

The morphological evolution of ion-beam-induced surface ripples has recently been extensively investigated, and several models of ripple growth based on continuum dynamical equations for the height of the interface have been proposed and numerically evaluated. These studies have revealed a rich variety of interesting new phenomena.[1–8] Four primary mechanisms have been considered for ripple formation including: sputtering, surface diffusion, redeposition, and viscous flow.[1–3,5,9] At the initiation point of surface ripple formation, a linear partial differential equation was developed in which only a first-order term in the slope was included. In this regime, the driving mechanism is the dependence of the sputtering yield on the local surface curvature. The orientation and wavelength of the ripples can be described by the Bradley and Harper (BH) model.[1] With increasing ripple slope for continuing bombardment, a second-order term in the slope was added and an associated nonlinear partial differential equation was developed.[2–4] In this regime, the nonlinear terms dominate and give rise to other surface morphologies such as roughening, coarsening, and saturation of ripples by either destroying existing ripples or generating a new rotated ripple structure.[2,10] Most of the morphological features induced by ion bombardment can be accounted for based on this nonlinear equation. However, recent experimental observations show that the existing models can only partially describe (or even contradict) the observed propagation of ripples. For example, for a Si (111) surface bombarded by 30 keV Ga ions, Habenicht *et al.*[11] found that the propagation direction of ripples on Si due to ion bombardment is opposite to that predicted by current models. The same result has been reported by Alkemade[5] for the ion bombardment of SiO_2. Additionally, Datta and Chini[12] found no shift in the ripples following the ion bombardment of diamond. Ripple propagation is an important phenomenon in its own right, but this aspect of ion-beam-induced surface modification has not been extensively studied.

A common feature of most models for ripple formation is the assumption of a smooth surface profile.[13] Under this assumption, the surface can be described in powers of derivatives of the ripple height, and thus, analytical results can be obtained based on Sigmund's theory.[1–3,14] For ripple propagation, the velocity can be calculated using the BH model in the linear regime.[1] This model was derived using an integral form of the sputtering yield given by Sigmund and a prescribed undulating shape of the surface under the small-slope approximation. Thermally induced surface diffusion was incorporated to balance the sputtering. Using linear analysis, a critical incident angle (around 65°) separating the propagation direction was obtained. When the incident angle is smaller than this critical value, the ripple moves against the projected ion beam direction; while when the incident angle is larger than this critical value, the ripple moves along the projected ion beam direction. This critical angle has, however, not been experimentally observed previously, and the experimental results, in fact, show movement taking place along the opposite direction relative to that predicted. Recently, a viscous flow term was added to the BH model to explain the propagation of surface ripples.[5] In this model, an amorphous layer undergoing viscous flow with a stress proportional to the layer thickness was suggested. Based on the Navier-Stokes relations, a nonlinear partial differential equation describing viscous flow induced by ion bombardment was derived. Linear analysis using first-order terms in the height shows that the viscous flow gives rise to an extra velocity that causes the ripples to move along the projected ion beam direction for all incident-beam angles. However, this approach is also only valid under the small-slope approximation, and it neglects the actual morphology of the ripples.

Investigations of ion-induced features with a large slope have been reported.[15–18] Barber *et al.*[18] proposed a geometrical construction to the predicted morphological evolution

during ion bombardment by employing an approach used in chemical etching. Nobes *et al.*[15–17] derived a shock-wave equation on the basis of the fact that different erosion by an ion beam along the curvature can lead to a slope change. Based on this model, Nobes *et al.*[15–17] successfully predicted many of the surface features induced by an ion beam, including the cone formation, the apex angle of the cone, and the evolution of a hemispherical trough. In a more recent analysis of the ion sputtering of steep surface features, Chen *et al.*[19] developed a shock-wave equation by making use of the classical theory of sputtering yield without using the small-slope approximation. By considering thermal diffusion, Chen *et al.*[19] found a stable slope for long-time bombardment consistent with that predicted by Barber *et al.*[18] and Nobes *et al.*[15–17] In Ar-ion-irradiated Si, Chini *et al.*[20] reported that ion-induced ripples have amorphous layers and that one side of the ripple is parallel to the ion beam direction. In addition, the formation of saw-tooth-like ripples has been discussed by Carter.[21]

In the present work, the morphological evolution of ion-beam-induced ripples on the $Cd_2Nb_2O_7$ pyrochlore surface formed by focused ion beam (FIB) bombardment is investigated. Through *in situ* experiments, terracelike ripples were found that consisted of relatively steep slopes. The slope and velocity of the terrace depended only on the incident ion beam angle, independent of the details of the ion bombardment process. Following the approach by Nobes *et al.*,[15–17] a partial differential equation was formulated for arbitrarily large slopes in which a shock wave was present. The terracelike ripples can, therefore, be understood in terms of the propagation of a shock front that "self-selects" a stable slope.

II. EXPERIMENTAL

The experiments were carried out using a FIB in a dual-beam instrument (FEI Nova 200 NanoLab). A single crystal of $Cd_2Nb_2O_7$ pyrochlore was irradiated in a vacuum of 2×10^{-7} mbar at room temperature. A 30 keV focused Ga^+ beam with a current of 5 nA was used for all of the ion beam experiments. The incident angle was varied from 35 to 65° to measure the relationship between the propagation velocity and incident angles. An ion fluence of $\sim 3 \times 10^{18}$ cm^{-2} was chosen as the high-fluence limit. The spot size of the 30 keV Ga^+ ion beam was 50 nm with an overlap of 50%. Each spot size was bombarded during 1 μs with a repetition time of 100 ms. The surface morphology was characterized by *in situ* scanning electron microscopy (SEM) and *ex situ* atomic force microscopy (AFM). AFM measurements were carried out in the tapping mode under ambient condition using phosphorus-doped Si cantilevers (Nanoscope IV).

III. RESULTS

In order to eliminate the effects of sample shift on the propagation of the ripples, ion bombardment was first performed on a single area of 30×30 μm^2 for 5 min—corresponding to an ion flux of 3.5×10^{15} s^{-1} cm^{-2}. One-sixth of the area was then covered, and the ion beam impacted the remainder of the surface for an additional 3 min

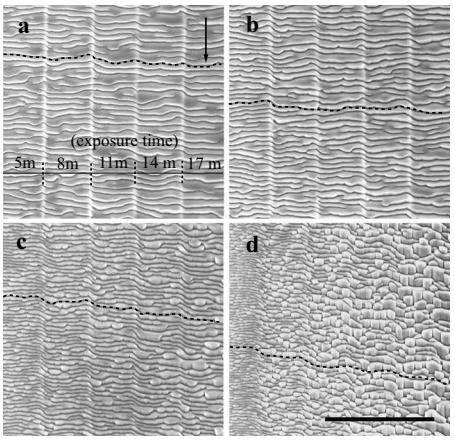

FIG. 1. SEM images showing the propagation of ripples with the ion beam at different incident angles. Five regions are shown in each image; the fluence is 1.04×10^{18} cm^{-2} for the left region (5 min) and increases by 6.24×10^{17} cm^{-2} (3 min) per region from the left to right. Dashed lines indicate the propagation of ripples, and the arrow is the projected ion beam direction. Incident angles are (a) 35, (b) 40, (c) 50, and (d) 60°. The scale bar is 10 μm. Note the ripple shifts along the projected ion beam direction with increasing fluence.

using the same flux. Subsequently, 2/6 of the area was covered, and bombardment of the remainder of the area was continued. This step was repeated until five regions were formed, each of which was subjected to a higher fluence (6.24×10^{17} cm^{-2}) than the previous area (Fig. 1). Thus, it was possible to accurately follow the relative movement of the ripples with increasing ion fluence in a single examination. For incidence angles ranging from 35 to 65°, the propagation direction is along the projected ion beam direction. This direction is in accordance with the observations reported by Alkemade[5] and Habenicht and Lieb[11] but is opposite to that predicted by existing models.[1–3]

Most of the common features of ripple evolution as a function of variations in the ion fluence for different materials in previous studies are shown in Fig. 1. These include a coarsening effect with an increase in the wavelength such that small ripples are effectively eliminated by merging together;[12,22] a transition from the perpendicular model (i.e., with the wave vector perpendicular to the ion beam direction) to a parallel mode at a fixed angle of incidence [Fig. 1(d)] (Ref. 10 and 22); the movement of the propagation along the projected ion beam direction regardless of the angle of incidence;[5,11] and a roughening effect.[7,21] As shown by dashed lines in Fig. 1, the propagation direction is always along the projected ion beam direction—although at low incidence, the magnitude of the shift of the ripples is small.

Figure 2 shows the relationship between the propagation of the ripples and the incident ion beam angle as obtained from Fig. 1. The average velocity was calculated over the entire image (50 fronts were counted for each image). Due to the coarsening of the ripples, only the fronts crossing neighboring regions (or several regions) are considered here. At a fixed flux, the velocity is stable with increasing bombardment time, but it increases with an increasing angle of incidence. The propagation velocity was found to be propor-

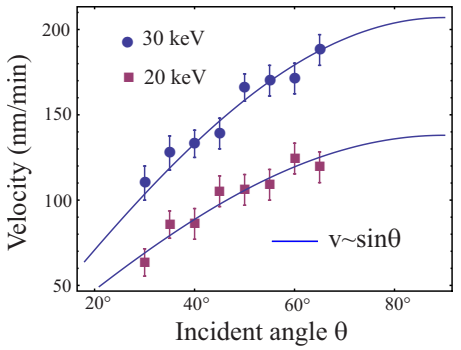

FIG. 2. (Color online) Dependence of the propagation velocity on incident angle at energy 30 and 20 keV. Flux is 3.5×10^{15} s^{-1} cm^{-2}.

tional to the sine of the angle of incidence. To study both flux and energy effects, experiments were performed using various fluxes and different energies. If the fluence is sufficiently large (i.e., larger than 1×10^{17} cm^{-2}), the dependence on the sine of the angle of incidence can be observed.

As noted above, most prior studies of ripple behavior have focused on the dynamic equations and ascribed the observed phenomena to the evolution of nonlinear terms. Microscopic details of the ripple profile have previously been overlooked, and the profile was assumed to be a smooth curve (i.e., without facets) with a small slope.[1,2] By taking high-magnification images along various viewing directions (Fig. 3), we find that terrace structures with steep slopes are, in fact, generated with increasing ion beam fluence. By rotating and tilting the sample [Figs. 3(a) and 3(b)], these characteristic structures can be identified via details that are not readily observable in images obtained at low magnification (Fig. 1). Moreover, by studying the orientation of the terraces, it was found that one surface of the terrace is parallel to the ion beam while the other is nearly perpendicular to the ion beam (Fig. 4). Parallel facets can be confirmed from images viewed along the beam direction [Fig. 4(a)]. Because one side of the structure cannot be observed along this direction, this side should be parallel to the ion beam. If a shadow area exists, as shown by Carter,[21] saw-tooth-like ripples will develop in which one side of the saw tooth is nearly parallel to the ion beam. When viewed from the direction perpendicular to the ion beam [Fig. 4(b)], the other side of the terrace (which is nearly perpendicular to the ion beam) can be observed. This relationship can also be confirmed by utilizing cross-sectional SEM images [see Fig. 4(c)] and AFM cross-sectional profiles [see Fig. 4(d)]. It was found that the terrace structure described above propagates over a large distance while preserving or even sharpening the characteristically steep slopes.

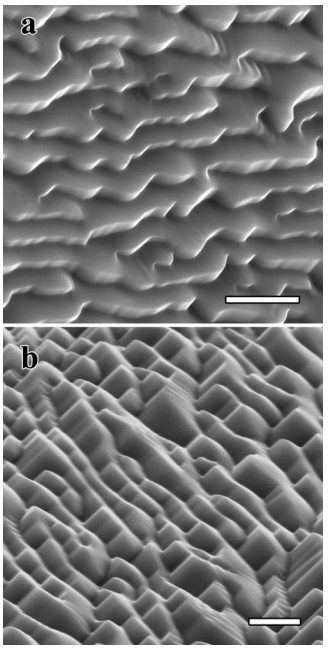

FIG. 3. SEM images showing the terracelike ripples induced at incident angles of (a) 45 and (b) 60°. The viewing directions are (a) tilt 20° relative to surface normal and (b) rotated 40° and tilted 30° relative to normal. The fluence is 6×10^{17} cm^{-2}. The projected ion beam before rotation and tilt is from top to bottom. Scale bar is 1 μm.

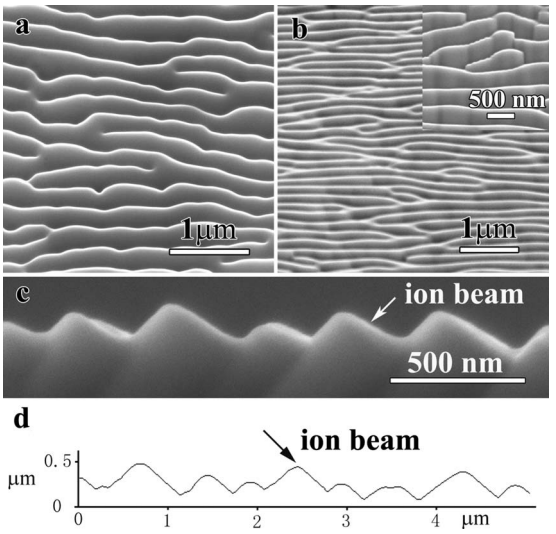

FIG. 4. SEM and AFM images showing the orientation of ripples related to ion beam direction. The SEM images are viewed from (a) parallel to ion beam and (b) perpendicular to ion beam. (c) Cross-sectional SEM image. (d) AFM cross-section profile. Energy at 30 keV, fluence of 6×10^{17} cm^{-2}, and incident angle at 45°. Inset shows the ripple induced at 65° with energy 30 keV and fluence of 2×10^{17} cm^{-2} viewed from direction perpendicular to ion beam.

Figure 5 shows the transition area between the effects due to the different ion beam fluences. As compared with Fig. 1, the enlarged images in Fig. 5 reveal additional details regarding the ripple growth. Only the perpendicular side of the ripples recedes while the other (parallel) side is not shifted. This arises because the sputtering yield is close to zero for the parallel side and only the perpendicular sides are sputtered. Further support for this process can be obtained from the images that are viewed from the directions either perpendicular or parallel to the ion beam [see the insets in Figs. 5(a) and 5(b)].

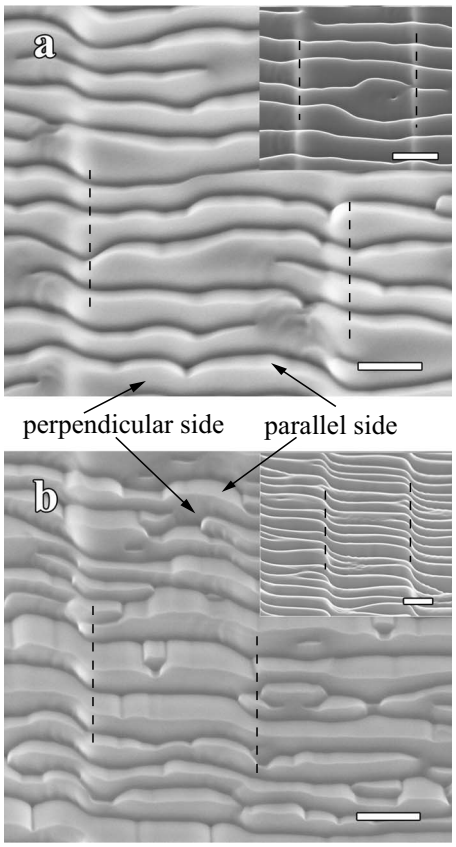

FIG. 5. Ripple evolution at different ion fluences (SEM images). High magnification image with a tilt at 15° relative to surface normal at incident angles (a) 40 and (b) 60°. The insets show SEM images viewed from direction (a) along ion beam direction and (b) perpendicular to ion beam direction. Only the perpendicular side is sputtered and recedes, but the parallel side does not shift for different fluences. Dashed lines show different fluence regions. From right to left the fluence increases by 6.24×10^{17} cm^{-2}. Scale bar is 1 μm.

IV. DISCUSSION

A. Steady-state topography induced by ion sputtering

At the initiation of the ripple formation process, the surface varies sufficiently smoothly so that the conditions for the validity of the BH model are satisfied. The ripple formation can then be described by a linear equation, and the corresponding ripple orientation and wavelength can be calculated directly by linear analysis. As the sputtering proceeds, due to curvature-dependent sputtering effects where the crest erosion is lower than that of the trough, the steep ripple slopes are generated. Hence, the model resulting from an expansion in gradients of the ripple height breaks down.

The explanation used to account for the deep slope formation observed in cone structures induced by ion beam bombardment can be applied to our experiments.[15–17] Following this approach, we can derive an equation for the ripple growth profile. Here we assume that the sputtering yield is only dependent on the incident-beam angle and that redeposition, viscous flow, and thermal diffusion are all negligible. As shown in Fig. 6, the coordinates are established

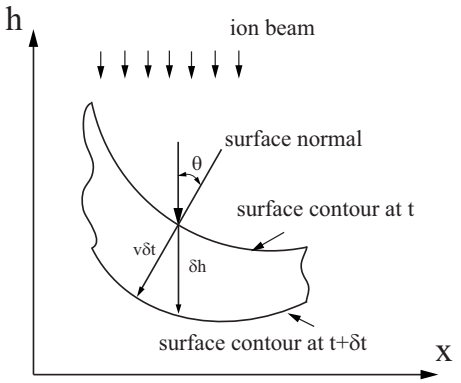

FIG. 6. Evolution of surface bombarded by ion beam. Ion sputtering rate direction is along the surface normal.

with the h axis parallel to the ion beam. For a two-dimensional slope, the rate can be determined by the sputtering yield. At a normal incidence of ion bombardment, sputtering occurs in a direction that is locally normal to the surface. The incident-beam angle θ is the angle measured from the ion beam direction to the surface normal. When the surface is removed by an ion beam with velocity v at time t, the decrease along the h axis is given by

$$\frac{\partial h}{\partial t} = -v\sqrt{1+p^2}, \tag{1}$$

where p is slope given by $p=\partial h/\partial x$. If we only consider sputtering yield, v is given by

$$v = \Omega I(\theta) Y(\theta), \tag{2}$$

where Ω is atomic volume, $I(\theta)$ is local ion flux, and $Y(\theta)$ is sputtering yield at incidence θ. The latter two terms are surface slope dependent. For normal bombardment $I(\theta)$ is given by

$$I(\theta) = \frac{I}{\sqrt{1+p^2}}, \tag{3}$$

where I is ion flux. A combination of Eqs. (1)–(3) gives

$$\frac{\partial h}{\partial t} = -\Omega I Y(\theta). \tag{4}$$

If we make derivative of Eq. (4) in terms of x, we have

$$\frac{\partial p}{\partial t} = -\Omega I \frac{\partial Y(\theta)}{\partial \theta} \cdot \frac{\partial \theta}{\partial x}. \tag{5}$$

The same equation has been derived previously by Nobes *et al.*[15–17] using a different approach. Using this equation, they explained the process of sharp cone formation and derived a relationship such that the apex angle of the cone is $\pi-2\theta_c$ where θ_c is the critical angle for which the sputtering is a maximum.[15–18] Equation (5) shows that the change in slope in terms of time depends on two terms: the change in the sputtering yield in term of the incident ion beam angle and the change in the incident angle in terms of the coordinates. For the case of the sputtering yield, as shown in Fig. 7(a),[23] it is well known that the sputtering yield increases

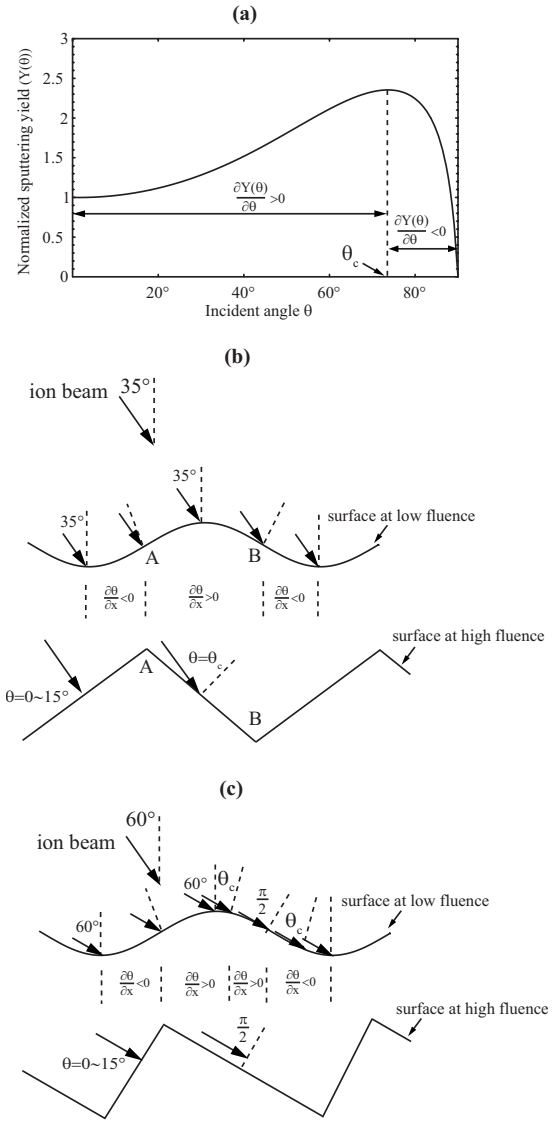

FIG. 7. Schematic illustration of the process of terracelike ripple formation. (a) The dependence of the sputtering yield on the incident angle and terracelike ripple formation with increasing of fluence at (b) 35 and (c) 60°. In (b), A shows smallest incident angle and B shows largest incident angle. In (c) critical incident angle (θ_c) and shadow area (starting at incident angle $\pi/2$) appear. Dashed lines show surface normal.

slowly for angles from 0 to around 70° and then decreases abruptly to zero at 90°. There is a maximum value of the sputtering yield for which $\partial Y(\theta)/\partial\theta=0$. Here we assume that the initial surface is a sinusoidal curve, and the change in local incidence with the coordinate is shown in Figs. 7(b) and 7(c). Because the signs of $\partial Y(\theta)/\partial\theta$ and $\partial\theta/\partial x$ are known for a given curve, we can determine the slope change during ion bombardment.

Under steady state $\partial p/\partial t=0$, we have $\theta=0$, $\theta=\pi/2$, or $\theta=\theta_c$, and the final slope is the slope that the local incident angle should be one of the three possible solutions at steady state $(0,90°,\theta_c)$. If we know the signs of $\partial Y(\theta)/\partial\theta$ and $\partial\theta/\partial x$, the increase or decrease in slope (i.e., the local incident angle) can be obtained. Hence, for a high-fluence limit,

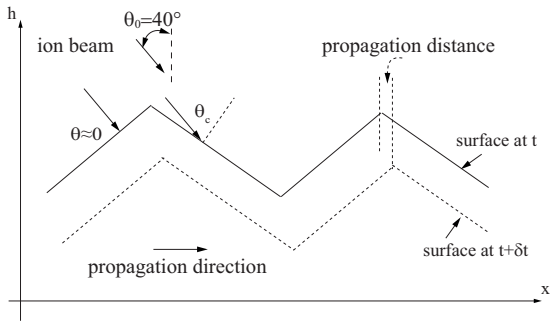

FIG. 8. Schematic illustration of the propagation of terracelike ripples. The competitive of local flux and sputtering yield leads to the propagation of ripples along projected ion beam direction.

a combination of three slopes can be obtained as shown by Nobes and Carter.[15–17] If the local incident angle $\theta<\theta_c$ (which means $\partial Y(\theta)/\partial\theta>0$), two conditions can be found: for $\partial\theta/\partial x>0$, slope p will decrease and consequently we have $\theta\rightarrow\theta_c$; another condition is $\theta\rightarrow 0$ for $\partial\theta/\partial x<0$. If the local incident angle $\theta>\theta_c$ [which means $\partial Y(\theta)/\partial\theta<0$], there are also two conditions: $\theta\rightarrow\pi/2$ when $\partial\theta/\partial x<0$ and $\theta\rightarrow\theta_c$ when $\partial\theta/\partial x>0$. At off-normal incidence, for simplicity, we rotate coordinates and let h be parallel to the ion beam direction. Under this condition, Eq. (5) does not change but the slope should be evaluated in the rotated coordinates. At low incident angle [Fig. 7(b)], condition $\theta<\theta_c$ is satisfied along the whole surface. We then have a steep surface with incidence $\theta=0$ for $\partial\theta/\partial x<0$ and $\theta=\theta_c$ for $\partial\theta/\partial x>0$. At high incidence [Fig. 7(c)], there exist points at which the off-normal beam is tangent to the curve on the surface, which means that no motion perpendicular to the ion beam can be induced by the ion beam, i.e., only planes either parallel or perpendicular to the ion beam incidence can be formed on the surface under the high-fluence limit. Therefore, parallel and perpendicular facets can be induced [Fig. 7(c)]. For a low incident angle, the length of the perpendicular surface is shorter than that of the parallel surface—while for a high incident angle, it is the reverse. These results are in good agreement with the experimental observations. The discontinuous points [for example, A and B in Fig. 7(b)] can be understood from the different sputtering yields: a peak position appears at point A because the sputtering yield is a minimum compared with the neighbors, while at point B, the sputtering is a maximum (i.e., for the largest incident angle), and a trough can be generated. Because the curve of the sputtering yield [as related to incident angle, see Fig. 7(a)] is so flat around $0\sim15°$, the incidence on the perpendicular side of terrace at steady state can be varied in a range of $\theta=0\sim15°$.

The ripple propagation velocity can also be explained from this particular shape. At low incidence ($\theta<45$), the maximum sputtering yield occurs on the slope (down slope) that is opposite to the ion beam [Fig. 7(b)]. As shown in Fig. 8, for the slope (up slope) that faces the ion beam, incident angle $\theta=0$, the flux is I, sputtering yield is Y (sputtering yield at $\theta=0$), and projected velocity along x axis is $v_x=\Omega I\sin\theta_0 Y$, where θ_0 is the angle between ion beam and global surface normal. For the slope that opposes the ion

beam, the flux is $I\cos\theta_c$, sputtering yield is $Y(\theta_c)$, and projected velocity along x axis is $v_x=-\Omega I\sin(\theta_c-\theta_0)\cos\theta_c Y(\theta_c)$. Therefore, the observed velocity is

$$v_p=\Omega I[\sin\theta_0 Y-\sin(\theta_c-\theta_0)\cos\theta_c Y(\theta_c)]. \quad (6)$$

If we use Sigmund's theory, $Y(\theta)=Y\cos^{-1}\theta$, which is valid at incident angle $\theta<60°$,[1,14] we have positive propagation velocity at $\theta>35°$ by assuming that $\theta_c=70°$.

At high incident angle ($\theta>45°$), we should consider the shadow effects [Fig. 7(c)]. Under these conditions, the sides of the terrace are either perpendicular or parallel to the ion beam. The velocity is

$$v_p=\Omega IY\sin\theta_0. \quad (7)$$

This result is also in good agreement with our experimental observations.

Note that, from the present results, the value of the velocity at low incidence also satisfies Eq. (7) (Fig. 2), and the incident angle on the slope that is opposite to the ion beam is close to $\pi/2$ (Fig. 5). However, from Fig. 7(b), the critical incident angle was predicted on the down slope. This means that sputtering alone cannot explain the parallel structure formation. For low incident angles, one needs to consider other mechanisms. It is known that linear curvature-dependent viscous flow and surface diffusion can give rise to surface smoothing resulting in a decrease in the angle between the facets from 70 down to 60° or less for the "down" slope.[9,24,25] However, if we assume that there is an amorphous layer on the surface of the substrate, ion impact can generate a local anisotropic deformation and plastic flow—resulting in a nonlinear curvature-dependent viscous flow and ripple formation.[26–28] Because this flow is a function of stress that depends on the thickness of the amorphous layer, the substrate can lead to an increased retardation of flow near the troughs relative to the crests of the surface. As a result, a shadowing area can be created, leading to parallel facet formation. Additionally, the incident angle 35° is the minimum angle for ripple formation. For a slope equal to 1 (the small-slope approximation is valid at slopes less than 1), at an incident angle of 35°, the local maximum incident angle can reach a value close to 80°. Hence, for the large slopes (larger than 1) we have considered here, it is reasonable to assume a tangent profile of the ripples relative to the ion beam, and as a consequence, only perpendicular and parallel facets can be created.

B. Shocks in ripples

Since the slope $p=\tan\theta$, Eq. (5) can be rewritten as

$$\frac{\partial\theta}{\partial t}+C(\theta)\frac{\partial\theta}{\partial x}=0, \quad (8)$$

where $C(\theta)=\Omega I\cos^2\theta\partial Y(\theta)/\partial\theta$. This form of the equation is found in many physical phenomena and typically results in discontinuities due to the interference between waves. Shocks (or rarefaction waves) result when these discontinuities occur. In an analogy to chemical etching, Barber *et al.*[18] employed the properties of shock waves to develop a geometrical approach to predicting surface morphologies induced by ion beams. Subsequently, Nobes *et al.*[15–17] derived nonlinear equations confirming that ion bombardment can give rise to the shock waves and thus lead to edge formation. In a recent analysis of surface morphology development induced by ion beams, a kinematic shock-wave formulation has also been derived by Chen *et al.*[19] to interpret the steep slope development. It is now believed that the formation of a large-slope surface morphology during ion beam etching may be understood in terms of the propagation of a shock front. The analytical solution to this shock-wave equation is quite difficult, but the development of the surface morphology can be constructed from this equation by plotting the trajectories as well as the etching depth as defined by the sputtering yield.[15–18,29,30] In order to understand step formation in ripples, we have applied geometrical construction to a sinusoidal surface at various incidence angles. This approach is based on the fact that surface development during ion bombardment can be described by a shock wave in which the orientation of the ion-etching trajectories can be well defined by the velocity of the surface in the normal direction. A program was written to draw trajectories from 100 equally spaced points on the initial sinusoidal surface according to the slope and local incident angle that is a function of the coordinates. The slope of the trajectories as derived by Carter *et al.*[17] is given by

$$\frac{dh}{dx}=\frac{\sin\theta\cos\theta(dY(\theta)/d\theta)-Y(\theta)}{\cos^2\theta(dY(\theta)/d\theta)}. \quad (9)$$

The continuous equation for sputtering yield as a function of incident angle was given by[23]

$$Y(\theta)=\cos\theta\exp\left(-\frac{a^2}{2\alpha^2}\cos^2\theta\right), \quad (10)$$

where a is average ion energy depth and α is ion energy straggling ($a^2/2\alpha^2=3.5$ was used in computer calculation). For initial curve $h=\sin x$, at off-normal incidence θ_0 (global incidence), we have $\theta=|-\theta_0+\pi+\arctan(\cos x)|$. Figure 9 shows the profiles for the sputtering of a sinusoidal surface at different incidences. The trajectories show the distance and direction of the recession of the initial surface. Each trajectory slope is constant, and the initial surface point will move along this line under ion etching. Equation (9) and sputtering yield [Eq. (10)] determine the slope and depth, respectively.[15,18,21] When two trajectories meet, an edge is produced, and the lines beyond the meeting point are erased. The distance between $t=0$ and $t=1$ in Fig. 9 shows that the down slope recedes faster than the up slope. With the change in down slope, the erosion rate on some points on the down slope becomes smaller. Facet structure is evident for long-term bombardment where the incident angles of about 0 and 75° on two sides of the terrace are developed, and the velocity of propagation is along the projected ion beam direction at both high and low incidences. Due to neglecting other effects such as viscous flow and redeposition, the parallel facet cannot be predicted. Figure 9 shows that, at the very beginning of the bombardment, ripples move against the projected ion beam direction for all incident angles, and after a critical time, the ripples move along the projected ion beam

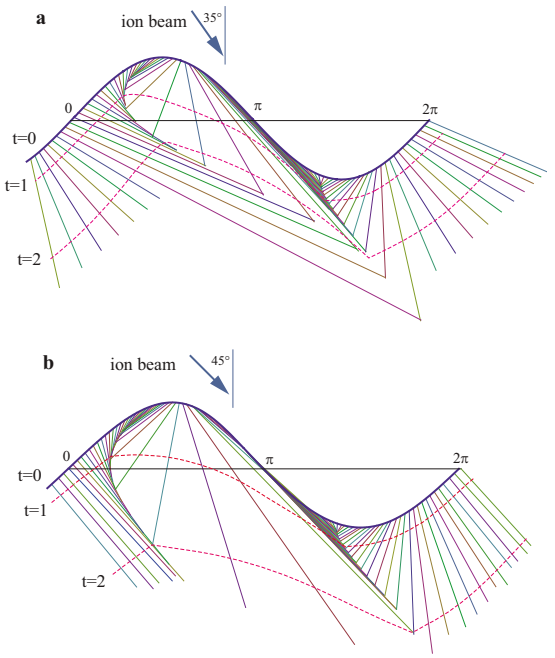

FIG. 9. (Color online) Geometrical construction of surface development subject to a uniform ion flux at incident angles (a) 35 and (b) 45°. The initial surface at time $t=0$ is sinusoidal. Dashed curves show the surface morphology after time $t=1$ and 2. Fine lines show the orientations of ion-etching trajectories. A facet structure forms due to the discontinuous slope.

direction. This result is consistent with predictions from the BH model. Therefore, the propagation of ripples at an early stage where the BH model is applicable cannot be detected, while observable ripple propagation takes place after facet formation at later time when the linear BH model breaks down.

An alternative explanation for ripple evolution is based on the earlier linear model work of BH and extended nonlinear models. Using Sigmund's theory,[14,31] the total number of sputtered atoms per unit area per unit time can be estimated by integrating the Gaussian distribution of energy on a prescribed shape of the surface. Equation (2) is then replaced by[2,14]

$$v = \Omega \int_{\Re} I(\mathbf{r}) Y(\mathbf{r}) d\mathbf{A}, \tag{11}$$

where $I(\mathbf{r})$ is a local flux, $I(\mathbf{r})d\mathbf{A}$ is the number of ions hitting on an area $d\mathbf{A}$, and $Y(\mathbf{r})$ denotes the sputtered atoms at original position ($r=0$) generated by an ion hitting the surface in a point $\mathbf{r}$. The integral is evaluated over the area $\Re$. This equation computes the sputtered atoms induced by the accumulated energy from different positions, i.e., curvature-dependent sputtering. Equation (2) only describes single-ion effects without any consideration of neighboring ion contributions and is valid for large-slope-dependent sputtering and the small curvature approximation.

Using Eq. (11), but without the small-slope approximation, Chen *et al.*[19] derived a partial differential equation and found that steep slopes with an incident angle of 76° can be induced by ion beams—consistent with our studies. Chen *et al.*[19] also showed that curvature-dependent sputtering can be ignored without a significant error, and the surface diffusion in which the diffusive fluxes are fourth order does not affect the slope and velocity.[19] Recently, redeposition and ion-induced viscous flow have been highlighted in the evolution of the surface morphology induced by ion beams.[5,9,32–34] The analytical equation for these two effects is, however, not well established.[32,35] In the present case, if we define redeposition as a damping term as shown by Facsko *et al.*[33] $\partial h/\partial t = -ch$, where h is surface height and c is a constant, in some cases, discontinuity cannot occurs.[30] This means that redeposition tends to smoothen the surface. In our experiment, the step structure can always be formed for the high-fluence limit, and thus, this term is not dominant. This may be due to the high-vacuum conditions that can lead to a small redeposition effect. Ion-induced viscous flow, as shown in section A, can, however, contribute to the formation of a parallel surface of terracelike ripples.

V. CONCLUSION

We have shown that terracelike ripples can be induced by ion beams after a long-term bombardment. The sides of the terraces are either parallel or perpendicular to the ion beam direction. This is accounted for based on slope-dependent sputtering rather than a curvature-dependent sputtering yield that has been widely used for the description of ripple formation. The velocity was measured and found to be proportional to the sine of the incident angle. The mechanism of formation for such a special shapes is treated by considering slope-dependent sputtering. Shock-wave phenomena were introduced to explain the observed terrace structure formation. Although this analysis is oversimplified in several respects, there is an encouraging qualitative agreement between the model predictions and the experimental results presented here.

ACKNOWLEDGMENTS

This work was supported by the Office of Basic Energy Sciences of the U.S. Department of Energy through Grant No. DE-FG02-02ER46005 and No. DE-FG02-97ER45656 Research at Oak Ridge National Laboratory is sponsored by the Division of Materials Sciences and Engineering, U.S. Department of Energy under Contract No. DE-AC05-00OR22725 with UT-Battelle, LLC.

*Corresponding author; lmwang@umich.edu

[1] R. Bradley and J. Harper, J. Vac. Sci. Technol. A **6**, 2390 (1988).
[2] R. Cuerno and A.-L. Barabási, Phys. Rev. Lett. **74**, 4746 (1995).
[3] M. Makeev, R. Cuerno, and A.-L. Barabási, Nucl. Instrum. Methods Phys. Res. B **197**, 185 (2002).
[4] J. Muñoz-García, M. Castro, and R. Cuerno, Phys. Rev. Lett. **96**, 086101 (2006).
[5] P. F. A. Alkemade, Phys. Rev. Lett. **96**, 107602 (2006).
[6] U. Valbusa, C. Boragno, and F. B. de Mongeot, J. Phys.: Condens. Matter **14**, 8153 (2002).
[7] G. Carter and V. Vishnyakov, Phys. Rev. B **54**, 17647 (1996).
[8] S. Rusponi, G. Costantini, C. Boragno, and U. Valbusa, Phys. Rev. Lett. **81**, 4184 (1998).
[9] E. Chason, T. M. Mayer, B. K. Kellerman, D. T. McIlroy, and A. J. Howard, Phys. Rev. Lett. **72**, 3040 (1994).
[10] S. Park, B. Kahng, H. Jeong, and A.-L. Barabási, Phys. Rev. Lett. **83**, 3486 (1999).
[11] S. Habenicht, K. P. Lieb, J. Koch, and A. D. Wieck, Phys. Rev. B **65**, 115327 (2002).
[12] D. P. Datta and T. K. Chini, Phys. Rev. B **69**, 235313 (2004).
[13] G. Carter, Phys. Rev. B **59**, 1669 (1999).
[14] P. Sigmund, Phys. Rev. **184**, 383 (1969).
[15] M. J. Nobes, J. S. Colligon, and G. Carter, J. Mater. Sci. **4**, 730 (1969).
[16] G. Carter, J. S. Colligon, and M. J. Nobes, J. Mater. Sci. **6**, 115 (1971).
[17] G. Carter, J. S. Colligon, and M. J. Nobes, J. Mater. Sci. **8**, 1473 (1973).
[18] D. J. Barber, F. C. Frank, M. Moss, J. W. Steeds, and I. S. T. Tsong, J. Mater. Sci. **8**, 1030 (1973).
[19] H. H. Chen, O. A. Urquidez, S. Ichim, L. H. Rodriquez, M. P. Brenner, and M. J. Aziz, Science **310**, 294 (2005).
[20] T. K. Chini, F. Okuyama, M. Tanemura, and K. Nordlund, Phys. Rev. B **67**, 205403 (2003).
[21] G. Carter, J. Appl. Phys. **85**, 455 (1999).
[22] A.-D. Brown, J. Erlebacher, W. L. Chan, and E. Chason, Phys. Rev. Lett. **95**, 056101 (2005).
[23] Q. M. Wei, K. D. Li, and L. M. Wang, J. Phys. D **41**, 172002 (2008).
[24] C. Herring, J. Appl. Phys. **21**, 301 (1950).
[25] W. W. Mullins, J. Appl. Phys. **30**, 77 (1959).
[26] C. Hajdu, F. Pászti, I. Lovas, and M. Fried, Phys. Rev. B **41**, 3920 (1990).
[27] G. Carter, Surf. Interface Anal. **25**, 952 (1997).
[28] A. Gutzmann, S. Klaumünzer, and P. Meier, Phys. Rev. Lett. **74**, 2256 (1995).
[29] R. Smith, G. Carter, and M. J. Nobes, Proc. R. Soc. London, Ser. A **407**, 405 (1986).
[30] G. B. Whitham, *Linear and Non-linear Waves* (Wiley-Interscience, New York, 1974).
[31] P. Sigmund, J. Mater. Sci. **8**, 1545 (1973).
[32] M. Castro, R. Cuerno, L. Vázquez, and R. Gago, Phys. Rev. Lett. **94**, 016102 (2005).
[33] S. Facsko, T. Bobek, A. Stahl, H. Kurz, and T. Dekorsy, Phys. Rev. B **69**, 153412 (2004).
[34] Q. M. Wei, J. Lian, W. Lu, and L. M. Wang, Phys. Rev. Lett. **100**, 076103 (2008).
[35] R. Gago, L. Vazquez, O. Plantevin, J. A. Sanchez-Garcia, M. Varela, M. C. Ballesteros, J. M. Albella, and T. H. Metzger, Phys. Rev. B **73**, 155414 (2006).